RSC Advances

Photocatalytic Hydrogen Generation from Water using a Hybrid of Graphene Nanoplatelets and Self Doped TiO$_2$-Pd

Farheen N. Sayed[a], R. Sasikala[a*], O.D. Jayakumar[a*], R. Rao[b], C.A. Betty[a], Anand Chokkalingam[c], R. M. Kadam[d], Jagnnath,[e] S. R. Bharadwaj[a], Ajayan Vinu[c] and A. K. Tyagi[a]

[a]Chemistry Division, Bhabha Atomic Research Centre, Trombay, Mumbai 400085, India

[b]Solid State Physics Division, Bhabha Atomic Research Centre, Trombay, Mumbai 400085,

[c]Australian Institute for Bioengineering and Nanotechnology (AIBN), The University of Queensland, Brisbane, QLD 4072, Australia

[d]Radio Chemistry Division, Bhabha Atomic Research Centre, Trombay, Mumbai 400085, India

[e]Technical Physics division, Bhabha Atomic Research Centre, Trombay, Mumbai 400085, India.

Corresponding authors email: sasikala@barc.gov.in, ddjaya@barc.gov.in

 Abstract:

Nanohybrids of self doped (Ti^{3+} doped or reduced TiO$_2$-TiO$_2$R) TiO$_2$-graphene nanoplatelets (TiO$_2$R-G) of different compositions are synthesized by a facile soft chemical method. A decrease of bandgap and improved visible light absorption is exhibited by TiO$_2$R-G. Based on current-voltage (I-V) measurements, it is concluded that the hybrid material possesses improved electron transport properties compared to TiO$_2$-R and pure TiO$_2$. A detailed characterization of the composites indicated that TiO$_2$-R exists as a dispersed phase on graphene nanoplatelets (Graphene). Among different compositions of the composites, the catalyst containing 3 weight % of graphene (TiO$_2$R-3G) shows enhanced photocatalytic activity for hydrogen generation from water compared to both TiO$_2$ and TiO$_2$-R. When Pd is used as co-

catalyst in this composite, a large increase in the activity is observed. The increased efficiency of the nanocomposite is attributed to factors like: (i) improved visible light absorption promoted by G and Ti^{3+} dopant (ii) increased lifetime of the charge carriers assisted by the enhanced electron transporting properties of G (iii) increased number of active sites for hydrogen evolution provided by Pd co-catalyst. This work highlights the role of TiO_2 based hybrid materials as efficient photocatalysts for solar energy utilization.

Introduction

Hydrogen is a clean fuel and its application for future energy needs is attractive as it does not generate any green house gas when burnt. Photocatalytic water splitting using solar radiation is one of the methods studied for hydrogen generation as both water and solar energy are renewable. For carrying out this reaction, development of suitable photocatalyst is needed, which can absorb visible light. Besides, the photo generated charge carriers should have sufficient lifetime so that the reaction can take place at an appreciable rate. TiO_2 is a widely studied photocatalyst as it is very stable and can be easily synthesized. A number of modifications of TiO_2 are reported like doping with cations,[1-4] anions[5-8] or both to make it visible light active.[9-13] Most of these doped catalysts show enhanced photocatalytic activity because the dopants modify the band structure of TiO_2 and improve the optical absorption property. Another method employed is to sensitize TiO_2 with dyes, which can absorb visible light and transfer the photo generated electrons to the conduction band of TiO_2.These electrons in the conduction band of TiO_2 can initiate the reduction of water.[14,15]

Another strategy used to improve the photocatalytic activity of TiO_2 is to make a composite with other semiconductors (SC) having suitable conduction band (CB) and valence band (VB) potentials. The photo generated electrons/holes from one SC can get transferred to the other, if band potentials are favorable, which can increase the lifetime of the charge carriers.

Thus, different composites of TiO_2 like TiO_2-SnO_2,[16,17] TiO_2-CdS,[18] TiO_2-ZrO_2,[19] TiO_2-$SrTiO_3$[20] etc. have been studied and reported to have improved photocatalytic activity.

Currently, researches are going on to investigate the role of graphene, a monolayer of graphite, in enhancing the photocatalytic activity of semiconductors. As graphene has certain unique properties like high surface area and high electrical conductivity, photoactive phases are embedded on it to increase the active surface area and to enhance the separation of photo generated charge carriers. Reports are available on graphene containing composites such as CdS-graphene,[21] Ag_3VO_4/TiO_2/graphene,[22] CdS-TiO_2-graphene,[23] TiO_2-graphene,[24] $ZnFe_2O_4$-ZnO-Graphene[25] etc., either for the photocatalytic hydrogen generation from water or for the photocatalytic degradation of organic pollutants present in water. Majority of these studies reported an enhanced photocatalytic activity due to the increased surface area and enhanced separation of charge carriers due to the presence of graphene in them. However, most of these studies have been on composites synthesized using reduced graphene oxide prepared by chemically reducing graphene oxide. Studies on composites utilizing pristine graphene/graphene nanoplatelets (G) are in scarce.

In the present work, we have synthesized a novel self-doped (Ti^{3+} doped) TiO_2-G nanocomposite by a facile new synthesis route and studied its photocatalytic activity for hydrogen generation from water in the presence of methanol as sacrificial reagent. The aim of the work is three fold: (i) to increase the surface area of self-doped TiO_2 by making a composite (ii) to modify the bandgap of TiO_2 by self-doping so that it can absorb visible light (iii) to enhance the separation of charge carriers by making a composite with graphene nanopaltelets. Detailed characterization of the composite was done and the observed activity is correlated with its physico-chemical properties.

Results and discussion

Powder XRD patterns of graphene nanoplatelets (G), TiO_2R and TiO_2R- G composites are shown in Fig. 1. Pure G shows a peak at $2\theta=26.5^o$, which can be assigned to the reflection from (002) plane of graphene.[26] The XRD pattern of TiO_2R is similar to that of TiO_2 and exists as anatase phase of TiO_2. All compositions of the composite samples show peaks corresponding to both TiO_2 and G indicating that they exist as separate phases. The BET surface area of graphene nanoplatelets, TiO_2R and TiO_2R-3G are 700, 75 and 190 m^2 g^{-1} respectively.

SEM and TEM images of TiO_2R-3G are shown in Fig. 2. SEM images of pure graphene nanoplatelets (Fig. 2(a)) show graphene of size ~5-10 µm. The TEM images of TiO_2R-3G (Fig. 2(b), 2(c) and 2(d)) show a dispersed phase of TiO_2 on graphene clearly. The particle size of the dispersed TiO_2R on graphene is found to be ~20-30 nm. HRTEM image (Fig. 2(e)) and SAED pattern (Fig.2(f)) confirmed that TiO_2 is in anatase phase. TEM and SAED pattern of TiO_2R are shown in Fig. S1 of electronic supplementary information (ESI). The particles appear to be of irregular shaped having a size of ~25 nm. The SAED pattern indicates that the sample has good crystallinity and it is polycrystalline in nature. The pattern could be indexed as anatase phase of TiO_2. This observation is in conformity with the XRD results of this sample.

Raman spectra of graphene nanoplatelets and TiO_2R-G composites are shown Fig.3. Raman bands at 151, 395, 514 and 638 cm^{-1} corresponding to $E_g(1)$, $B_{1g}(1)$, $A_{1g}+B_{1g}$ (2) and $E_g(3)$ vibrational modes of anatase TiO_2 are seen for all TiO_2R-G composites (Fig. 3A).[27, 28] Pure graphene nanoplatelets shows (Fig.3B) an intense Raman band at 1583 cm^{-1} corresponding to the G band, which arises due to the in plane vibration of sp^2 bonded C atoms (phonon E_{2g} mode).[29-31] A small peak seen at 1364 cm^{-1} (D band) suggests that some small amount of defects or sp^3 carbon atoms are present in this graphene.[29-31] The positions of D and G bands, their full width at half

maximum (FWHM) and the intensity ratio of D and G bands (I_D/I_G) of graphene and TiO_2R-G composites are given in Table 1 (S2) of ESI. The spectra of the composites are clearly different from that of pure graphene nanoplatelets and a peak broadening as well as a shift in the peak positions are observed for all composites. There is a marked increase in the ratio of relative intensity I_D/I_G from 0.3 in graphene to 1.4 in 3G. This significant change in the peak positions, shape and intensity of the G and D peaks suggests that there is a strong interaction between graphene and TiO_2R.

Chemical state of C, Ti and O in these composites was investigated by XPS. Fig. 4A and 4B show the Ti 2p, O 1s and C 1s XPS of TiO_2R and TiO_2R-3G respectively. The Ti $2p_{3/2}$ and Ti $2p_{1/2}$ peaks of TiO_2R are seen at BE values of 457.9 and 463.5 eV, respectively. The corresponding values for TiO_2R-3G samples are at 457.7 and 463.4 eV. Spectra of unreduced TiO_2 along with TiO_2R and TiO_2R-3G are shown in Fig. S3 of ESI to check whether there is any significant shift in the peak position of reduced samples with respect to unreduced TiO_2. Unreduced TiO_2 showed the Ti $2p_{3/2}$ peak at a BE of 458.1eV, which is comparable to the value reported for Ti^{4+} in TiO_2 (458.7 eV).[32, 33] Thus, it is seen that there is no considerable change in the Ti $2p_{3/2}$ peak positions of unreduced and reduced samples. O 1s spectra of TiO_2R and the composite were fitted into two peaks. The lower BE peak is attributed to the Ti^{4+}-O bonding of TiO_2.[34] The second peak seen around 531 eV can be assigned to adsorbed water on the surface or due to Ti^{3+}-O bond.[34, 35] C1s spectra of all samples showed an intense peak around 284.5 eV corresponding to the C-C bonding of graphitic carbon.[27] This confirms that graphene is in a reduced form and no graphene oxide is present in the composite samples. A very low intense peak is seen around 288 eV, which can be attributed to carbonate species adsorbed on the surface.[27] The reduced TiO_2 also showed the presence of carbon as it was synthesized from

organic precursors. As we have used hydrazine for the reduction of TiO_2, the possibility of N getting doped on the surface was explored. The N 1s spectra of all samples are shown in Fig. S4 of ESI. The absence of peak in the region 390-410 eV confirms that the surface of these samples do not contain any bonded N or nitrogen containing species.[27]

As XP spectra did not give any conclusive evidence for the presence of Ti^{3+}, EPR spectra of the reduced as well as unreduced samples were recorded. The presence of Ti^{3+} and other paramagnetic species like O_2^- in TiO_2R, TiO_2R-3G and TiO_2R-5G were examined by recording electron paramagnetic resonance at room temperature and at 100 K. It may be noted that the EPR is insensitive to Ti^{4+}, and hence no EPR signal is observed in unreduced samples (Fig 5a). EPR spectrum of TiO_2-R sample (Fig. 5b) showed a signal at g = 1.985 which was attributed to presence of Ti^{3+} center in a distorted octahedral symmetry of oxygen in this sample.[36] The concentration of Ti^{3+} is measured by comparing the integrated ares of EPR signal due to Ti^{3+} in reduced TiO_2 (TiO_2-R) and $CuSO_4$ $5H_2O$ sample and is estimated to be around 0.09% (by weight) in TiO_2-R. It is believed that surface Ti^{3+} would adsorb atmospheric oxygen which would be reduced to O_2^- (g_1=2.025, g_2=2.009 and g_3=2.003). However, in the present case, no signal was observed at these g values. Whereas, room temperature EPR spectra of TiO_2R-G composites (TiO_2R-3G and TiO_2R-5G) showed a relatively narrow peak at g ca 1.99 having line width of $\Delta H_{pp} \approx 50$ G which was attributed to Ti^{3+} and this signal is superimposed on an intense broad peak ($\Delta H_{pp} \approx 1500$ G) which can be attributed to the presence of graphene. The electronic structure and magnetic properties for layered graphene synthesized by chemical vapor deposition has been investigated previously by EPR.[37] The broad signal in their measurements was dependent strongly on annealing temperature and was attributed to presence of localized spins in graphene nanoribbons.

UV-visible absorption spectra of TiO_2, reduced TiO_2 and composites are shown in Fig. 6A. Increased visible light absorption is seen for all composite samples and for TiO_2R as compared to pure TiO_2. A red shift of the absorption edge is seen for all samples compared to pure TiO_2 and it is the highest for TiO_2R-3G. Plots of transformed Kubelka-Munk function against energy to calculate the bandgap of different samples are shown in Fig. 6B. It is seen that the bandgap of TiO_2R has decreased (3.04 eV) as a result of incorporation of Ti^{3+} in TiO_2. The presence of Ti^{3+} creates anion vacancies in the lattice and generates defect levels within the bandgap of TiO_2. This vacancy induced band can overlap with the CB of anatase phase TiO_2 and decrease the band gap.[4,38] The bandgap of all composites were less than that of pure TiO_2 and the values are 3.22, 3.04, 2.66 and 3.09 eV for TiO_2, TiO_2R, TiO_2R-3G and TiO_2R-5G, respectively.

Electrical properties of TiO_2/modified TiO_2 have been studied by conducting I-V measurements and the characteristics are shown in Fig. 7. Inset shows the schematic of the pellet and the silver contacts used for I-V measurements. While the I-V characteristics for TiO_2 showed ohmic behavior, modified TiO_2 (both TiO_2R and TiO_2R-3G) showed non-ohmic behaviour. The non-ohmic behavior of I-V characteristics indicates that, there is a difference in the electron affinity of TiO_2, TiO_2R and TiO_2R-3G. It may be seen from the figure that both TiO_2R and TiO_2R-3G show a significantly increased current compared to undoped TiO_2. The increased current and the non-ohmic behavior shown by the reduced TiO_2 in the I-V experiment can be attributed to the increased number of anion vacancies, which results in shallow levels below the conduction band. The shallow levels allow the charge separation before e-h recombination. The Shcotky barrier between TiO_2R and graphene can cause the non-ohmic behaviour shown by TiO_2R-G. It is known that Schotky barrier gets formed between graphene and ZnO nanowires[39,40] The significant current enhancement observed for TiO_2R-G compared to TiO_2R can be attributed

to the efficient electron transfer from the conduction band of TiO_2R to the graphene. TEM images (Fig. 2(b-d)) clearly show that TiO_2R is densely surrounded by 2D- graphene indicating large area contact surface. The large contact surface and the excellent conducting property of G promote efficient electron transfer from TiO_2R to the graphene improving the charge seperation and thus the lifetime of carriers.

Photocatalytic activity of TiO_2, TiO_2R and the composites are shown in Fig. 8A. It can be seen that the photocatalytic activity of TiO_2R is more than that of pristine TiO_2. Addition of graphene nanoplatelets (graphene) increases the photocatalytic activity of TiO_2R and the optimum concentration of graphene is found to be 3wt%. Further increase in the concentration of graphene does not increase the activity of TiO_2R. There exists an optimum concentration of graphene, which can enhance the photocatalytic activity of a semiconductor.[41] When the concentration is low, the contact established between the photoactive material and graphene is not sufficient. The decreased activity with increased concentration of graphene is attributed to a 'shielding effect', which results in the masking of TiO_2 from the incident light and decreases the light absorption. Effect of Pd co-catalyst on the activity of TiO_2R-3G, which showed the highest activity among the composite sample, was studied and the result is shown in Fig.8B. A significant increase in the amount of hydrogen generated is observed in the presence of Pd and a hydrogen evolution rate of 288 μmoles g^{-1} h^{-1} is obtained using this catalyst. The sample is used repeatedly for photocatalysis experiment and found that the activity is almost same during repeated cycles indicating that the sample is stable. Photocatalytic activity for the TiO_2R-3G sample for repeated cycle is shown in Fig. S5 of ESI.

A direct comparison of the hydrogen generation rate of the present work with that of reported values is inappropriate as the experimental conditions such as the source of light,

irradiated area etc. are different in each experiment. However, some reported results are presented here, which can give an idea about how good our photocatalyst is when compared with the reported ones. It is reported[42] that N doped TiO_2-Graphene composite under visible light irradiation produced hydrogen at a rate of 112 μmoles g^{-1} h^{-1}. A composite of TiO_2-reduced graphene oxide[43] showed an activity of 740 μmoles g^{-1} h^{-1} under UV-visible light of Xeonon arc lamp whereas a composite of TiO_2-MoS_2-graphene[44] generated hydrogen at the rate of 2066 μmoles g^{-1} h^{-1} under UV irradiation. A TiO_2 (P25)-graphene system[45] showed a hydrogen generation rate of 108 μmoles g^{-1} h^{-1} under UV-visible light of Xenon arc lamp and a TiO_2-RGO composite[46] produced hydrogen at a rate of 500 μmoles g^{-1} h^{-1} under UV irradiation. It may be noted that in all cases except the N-doped TiO_2[42], UV or UV-visible light was used for the experiment. When compared with the N doped TiO_2-graphene composite, which used visible light, our catalyst showed improved activity.

The enhanced photocatalytic activity of Pd-TiO_2R-3G can be attributed to a synergistic effect of Ti^{3+} dopant, graphene and Pd in increasing the charge separation in the composite system. The presence of Ti^{3+} creates anion vacancies in TiO_2 which can enhance the charge separation in the doped system.[47, 48] Graphene is well known for its excellent electron accepting and transporting properties.[49] Hence, the photogenerated electron from TiO_2R, which is having an intimate contact with graphene as seen from the TEM and Raman studies, can be immediately conducted away from TiO_2R minimizing the recombination of electrons and holes. A schematic illustration of the charge separation process occurring in the composite is shown in Fig. 9. The H^+ generated can combine with the electrons in graphene liberating hydrogen gas as the reduction potential of graphene/graphene$^-$ is more negative than the reduction potential of H^+/H_2.[49] The significantly high increase in the photocatalytic activity in the presence of Pd co-

catalyst is due to the interfacial transfer of electrons from the composite to the Pd metal. The noble metal co-catalyst acts as an electron sink, enhances the charge separation and increases the availability of electrons for H^+ reduction.[50]

Another reason for the increased photocatalytic activity of the composite is due to the increased visible light absorption as compared to pure TiO_2. Both Ti^{3+} and graphene play roles in enhancing the visible light absorption of TiO_2R-3G composite. Introduction of graphene can modify the band structure of TiO_2 due to a chemical interaction of TiO_2R and graphene forming Ti-O-C bonding, which increases the light absorption to extended visible region.[51] It may be recalled that a strong interaction between TiO_2R and graphene has been indicated by the Raman spectra of these samples.

Experimental

To synthesize TiO_2, 3 ml of Ti-isopropoxide (Sigma Aldrich, 99.9%) was added drop wise to 20 ml of isopropyl alcohol (Sigma Aldrich, 99.9%), followed by addition of 1 ml of distilled water. The white precipitate obtained was constantly stirred for 1h at 50 ^{o}C. The mixture was then evaporated to dryness. The powder thus obtained was heated at 450 ^{o}C for 2 h in air. The sample was then washed with distilled water and dried at room temperature. The dried product was again heated at 450 ^{o}C for 2 h in air.

For the preparation of composites with different ratios of graphene nanoplatelets (research grade, grade 4, < 5 nm thick, < 4 layers, obtained from commercial sources in Singapore) (1.0, 3.0, and 5.0 weight% of graphene with TiO_2), calculated amount of graphene nanoplatelets was added in 20 ml of isopropyl alcohol which was sonicated followed by stirring at 50 ^{o}C for 30 min. To this, 3 ml Ti-isopropoxide was added drop wise followed by the same procedure used for the pristine sample.

To synthesize TiO_2R and TiO_2R-G composites (TiO_2R-xG, where x=1.0, 3.0 and 5.0), all the samples were reduced in ethylene glycol medium, using hydrazine hydrate. The reduction was done at 180 ^{o}C for 2 h. Hydrazine is a well known reducing agent. The NH_2 group can react with the oxygen of TiO_2 forming water, N_2 and reduced TiO_2 as shown below.

$$TiO_2 + H_2N\text{-}NH_2 \rightarrow Ti^{4+(3+)}O_{2\text{-}x} + xH_2O + N_2$$
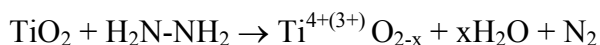
The product was separated and dried followed by heating in argon atmosphere at 450 ^{o}C for 2 h. Palladium as co-catalyst was loaded on TiO_2R-3G ($PdTiO_2R$-3G) by a wet impregnation method. Required amount of palladium chloride (0.5% by weight of the catalyst) was dissolved in distilled water and the powder was dispersed in it. The mixture was evaporated to dryness under constant stirring. The powder was photo reduced by suspending in water-methanol mixture (4:1 ratio) and exposing to UV-visible light of Xenon arc lamp (300 watts, Hamamatsu) for 4 h. The sample was removed from the solution, washed with acetone and dried under ambient conditions.

Characterization

Powder X-ray diffraction (XRD) patterns of these samples were recorded using a Philips PW1820 X-ray diffractometer coupled with a PW 1729 generator, which was operated at 30 kV and 20 mA. Graphite crystal monochromator was used for generating monochromatic CuK$_\alpha$ radiation. Surface area of the samples was measured using Brunauer, Emmett and Teller (BET) method employing nitrogen as the adsorbing gas. Transmission electron microscopy (TEM), high resolution TEM (HRTEM), selected area electron diffraction (SAED) and energy dispersive X-ray spectroscopy (EDXS) analyses were carried out using a JEOL JSM 2100 instrument operating at an accelerating voltage of 200 kV. The sample preparation for HRTEM imaging involved sonication in ethanol for 5 minutes followed by deposition on a copper grid. Raman

spectra were recorded using 532 nm line from a diode-pumped Nd-YAG laser (power 15 mW) focused to a spot size of about 20 μm. The scattered light was analyzed using a home-built 0.9 m single monochromator coupled with super notch filter and detected by a cooled charge couple device (CCD, Andor technology). The entrance slit was kept at 50 μm, which gave a resolution limited line width of 3 cm^{-1}. UV-visible diffused reflectance spectra (UV-Visible DRS) of all samples were recorded using a Jasco (model V-670) spectrophotometer equipped with an integrating sphere accessory. Barium sulfate was used as reference for recording the reflectance spectra. XPS studies were carried out in a VG Microtech electron spectrometer using Mg-K$_\alpha$ X-rays (hν= 1253.6 eV) as the primary source of radiation. Chamber pressure was maintained at 1×10^{-9} torr. Appropriate correction for charging effect was made with the help of C 1s signal appearing at 284.5 eV. The peaks were fitted using nonlinear square method by convolution of Lorentzian and Gaussian functions. EPR spectra were recorded by using EMX 1843 system operated at X band frequency (9.5 GHz). DPPH was used for calibration of g values. Approximately 50 mg of sample was placed in quartz tube and spectra were recorded under identical spectrometer settings. For the current-voltage (I-V) measurements the Potentiostat Parstat 273, was used. For the electrical contacts, silver dots (1 mm dia) were deposited on sample pellets on one side using silver ink (obtained from Electrulobe, UK).

Photocatalytic activity was studied in a tubular glass (pyrex) reactor using day-light fluorescent lamps as source of radiation. Details of the reactor and irradiation chamber are given in the ESI (S6) and in our earlier publications.[52, 53] The emission profile of the fluorescent lamp is given in Fig.S7 (ESI). Fifty milligram of sample was kept in contact with water (20 ml) containing methanol (5 ml) as sacrificial reagent under constant stirring. The reactor was flushed with argon gas before irradiation. After every one hour, the gas mixture in the reactor was

analyzed using a gas chromatograph (Chromatography and Instruments company, GC 2011) equipped with molecular sieve 5A column and thermal conductivity detector. The intensity of the light source was measured using a calibrated precision light meter (model cal-Light 400) and was found to be 69000 lux.

Conclusions

Self doped TiO_2-G composites show enhanced photocatalytic activity for hydrogen generation from water. The composite samples show improved visible light absorption due to the modification of the band structure of TiO_2 by Ti^{3+} and graphene. TiO_2R-G sample exhibits excellent electron transport properties compared to pure TiO_2. The improved photocatalytic activity of the composite is attributed to enhanced visible light absorption, large surface area and increased charge separation occurring in this system. Both graphene and Pd act as co-catalysts, which further increase the photocatalytic activity of Ti^{3+} doped TiO_2 further by facilitating the interfacial transfer of electrons from the photocatalyst to graphene and Pd resulting in the availability of large number of electrons for H^+ reduction.

References

1   C. Wang, C. Bottcher, D. W. Bahemann and J. K. Dohrmann, *J. Mater. Chem*., 2003, **13**, 2322.

2   R. Sasikala, V. Sudarsan, C. Sudakar, R. Naik, T. Sakuntala and S. R. Bharadwaj, *Int. J. Hydrogen Energy,* 2008**, 33**, 4966.

3   S. Murcia-Lopez, M.C. Hidalgo and J.A. Navio, *Appl.Catal. A: General*, 2011, **404**, 59.

4   R. Sasikala, V. Sudarsan, C. Sudakar, R. Naik, L. Panicker and S.R. Bharadwaj, *Int. J. Hydrogen Energy*, 2009, **34**, 6105.

5   O. D. Jaykumar, R. Sasikala, C. A. Betty, A. K. Tyagi, S. R. Bharadwaj, U.K. Gautam, P. Srinivasu and A. Vinu, *J. Nanosci. Nanotech*., 2009, **9**, 4663.

6   K. Lv, H. Zuo, J. Sun, K. Deng, S. Liu, X. Li and D. Wang, *J. Hazard. Mater*., 2009, **161**, 396.

7   S. Yin, K. Ihara, Y.Aita, M. Komatsu and T. Sato, *J. Photochem. Photobiol. A:Chem*., 2006, **179**, 105.

8   K. A. Michalow, D. Loginowich, A. Weidenkaff, M. Amberg, G. Fortunato, A. Heel, T. Graule and M. Rekas, *Catal. Today*, 2009, **144**, 7.

9   F. N. Sayed, O. D. Jayakumar, R. Sasikala, R. M. Kadam, S. R. Bhradwaj, L. Kienle, U. Schürmann, S. Kaps, R. Adelung, J. P. Mittal and A. K. Tyagi, *J. Phys. Chem. C*, 2012, **116**, 12462.

10   T. Ohno, Z. Miyamoto, K. Nishijima, H. Kanemitsu and F. Xueyuan, *Appl. Catal. A: General*, 2006, **302**, 62.

11   C.Liu, X. Tanga, C. Mo and Z. Qiang, *J. Solid State Chem*., 2008, **18**1, 913.

12   R. Sasikala, A.R. Shirole, V. Sudarsan, Jagannath, C. Sudakar, R. Naik , R. Rao and S.R. Bharadwaj, *Appl. Catal. A: General*, 2010, **377**, 47.

13   A. Charanpahari, S.S. Umare, S.P. Gokhale, V. Sudarsan, B. Sreedhar and R. Sasikala, *Appl.Catal. A: General*, 2012, **443– 444**, 96.

14   Z. Jin, X. Zhang, Y. Li, S. Li and G. Lu, *Catal. Commun*. 2007, **8**, 1267.

15   W. Kim, T. Tachikawa, T. Majima and W. Choi, *J. Phys. Chem. C*, 2009, **113**, 10603.

16   R. Sasikala, A. Shirole, V. Sudarsan, T. Sakuntala, C. Sudakar, R. Naik and S.R. Bharadwaj, *Int. J. Hydrogen Energy*, 2009, **34**, 3621.

17   M. Maeda and K. Hirota, *Appl Catal A: General*, 2006, **302**, 305.

18   V. M. Daskalaki, M. Antoniadou , G. L. Puma, D. I. Kondarides and P. Lianos, *Environ. Sci. Technol.* 2010, **44**, 7200.

19   R. Sasikala, A.R. Shirole, V. Sudarsan, V.S. Kamble, C. Sudakar, R. Naik, R. Rao and S.R. Bharadwaj, *Appl. Catal. A: General***,** 2010, **390**, 245.

20   J. Ng , S. Xu , X. Zhang , H. Y. Yang and D. D. Sun, *Adv. Funct. Mater.*, 2010, **20**, 4287.

21   N. Zhang, M. Q. Yang Z. R. Tang, and Y. J. Xu, *J. Catal.*, 2013, **303**, 60.

22   J. Wang, P. Wang, Y. Cao, J. Chen, W. Li, Y. Shao, Y. Zheng and D. Li, *Appl. Catal. B: Environmental,* 2013, **136– 137**, 94.

23   T. Lv, L. Pan, X. Liu, T. Lu, G. Zhu, Z. Suna and C. Q. Sun, *Catal. Sci. Technol.*, 2012, **2**, 754.

24   Y. Wang, R. Shi, J. Lin and Y. Zhu, *Appl. Catal. B: Environmental,* 2010, **100**, 179.

25   L.Sun, R. Shao, L. Tang and Z. Chen, *J. Alloys Comp.*, 2013, **564**, 55.

26   G. Wang, J. Yang, J. Park, X. Gou, B. Wang, H. Liu and J. Yao, *J. Phys. Chem. C*, 2008, **112**, 8192.

27   X. Yang, C. Cao, L. Erickson, K. Hohn, R. Maghirang and K. Klabunde, *J. Catal*., 2008, **260**, 128.

28   M. Gotic, M. Ivanta, S. Popovic, S. Music, A. Turkovic and K. Furic, *J. Raman Spectrosc*., 1997, **28**, 555.

29   A. C. Ferrari, J. C. Meyer, V. Scardaci, Casiraghi, M. Lazzeri, F. Mauri, S. Piscanec, D. Jiang, K. S. Novoselov, S. Roth and A. K. Geim, *Phys Rev Lett*.,   2006, **97,** 187401.

30   Shuyan Song, Wei Gao, Xiao Wang, Xiyan Li, Dapeng Liu, Yan Xing and Hongjie Zhang, *Dalton Trans*., 2012, **41**, 10472.

31   Z. Sun, Z. Yan, J. Yao, E. Beitler, Y. Zhu and J. M. Tour, *Nature*, 2010, **468**, 549.

32   K. A. Michalow, D. Logvinovich, A. Weidenkaff, M. Amberg, G. Fortunato, A. Heel, T. Graule, and M. Rekas, *Catalysis Today*, 2009, **144**, 7.

33   Y. Huo, Y. Jin, J. Zhu and H. Li, *Appl. Catal. B: Environmental***,** 2009, **89**, 543.

34   Y. Wang, M. Zhong, F. Chen and J. Yang, *Appl. Catal. B: Environmental*, 2009, **90**, 249.

35   M. Grodzicki, R. Wasielewski, P. Mazur, S. Zuber and A. Ciszewski, *Optica Applicata*, 2013, **XLIII**, 99.

36   F. Zuo, L. Wang, T. Wu, Z. Zhang, D. Borchardt and P. Feng, *J. Am Chem . Soc*., 2010, **132**, 11856.

37   V. L. Joseph Joly, M.Kiguchi, S-J. Hao, K. Takai, T. Enoki, R. Sumii, K. Amemiya, H. Muramatsu, T. Hayashi, Y. A. Kim, M. Endo, J. C. Delgado, F. López-Urías, A. B. Méndez, H. Terrones, M. Terrones and M. S. Dresselhaus, *Physical review B*, 2010, **81**, 245428.

38   I. Justicia, P. Ordejon, G. Canto, J. L. Mozos, J. Fraxedes and G. A. Battiston, *Adv. Mater*., 2002, **14**, 1399.

39 Y. Ye, L. Gan, L. Dai, H. Meng, F. Wei, Y. Dai, Z. J. Shi, B. Yu, X. F. Guo and G. G. Qin, *J. Mater. Chem*., 2011, **21**, 11760.

40 S. S. Lin, B. G. Chen, W. Xiong, Y. Yang, H. P. He and J. Luo, *Optics Express*, 2012, **A706**, 20 (S5).

41 Q. Li , B. Guo , J. Yu , J. Ran , B. Zhang , H. Yan and J. R. Gong , *J. Am. Chem. Soc*., 2011, **133**, 10878.

42 F. Pei, Y. Liu, S. Xu, J. Lu , C. Wang and S. Cao, *Int. J. Hydrogen Energy*, 2013, **38**, 2670.

43 W. Fan, Q. Lai, Q. Zhang and Y. Wang, *J. Phys. Chem. C*, 2011, **115**, 10694.

44 Q. Xiang, J. Yu and M. Jaroniec, *J. Am. Chem. Soc*., 2012, **134**, 6575.

45 X. Zhang, Y. Sun, X. Cui and Z. Jiang, *Int. J. Hydrogen Energy*, 2012, **37**, 811.

46 J. Shen, Y. Long, T. Li, Min Shi, N. Li and M. Ye, *Mater. Chem. and Phy*., 2012, **133**, 480.

47 L. Liu, F. Gao, H. Zhao and Y. Li, *Appl Catal B: Environmental*, 2013, **134– 135,** 349.

48 H. H. Lo, N. O. Gopal and S.C. Ke, *Appl. Phys. Lett*., 2009, **95**, 083126.

49 G. Xie , K.Zhang , B. Guo , Q. Liu , L. Fang and J. R. Gong, *Adv. Mater*., 2013, **25**, 3820.

50 P.V. Kamat, *J. Phys. Chem. C.* 2007, **111**, 2834.

51 H. Zhang, X. Lv, Y. Li, Y. Wang and J. Li, *ACS Nano*, 2010, **4**, 380.

52 R. Sasikala, A. R. Shirole, V. Sudarsan, K. G. Girija, R. Rao, C. Sudakar and S. R. Bharadwaj, *J. Mater. Chem*., 2011, **21**, 16566.

53 R. Sasikala , A. R. Shirole and S. R. Bharadwaj, *J. Colloid Interface Sci*., 2013, **409**, 135.
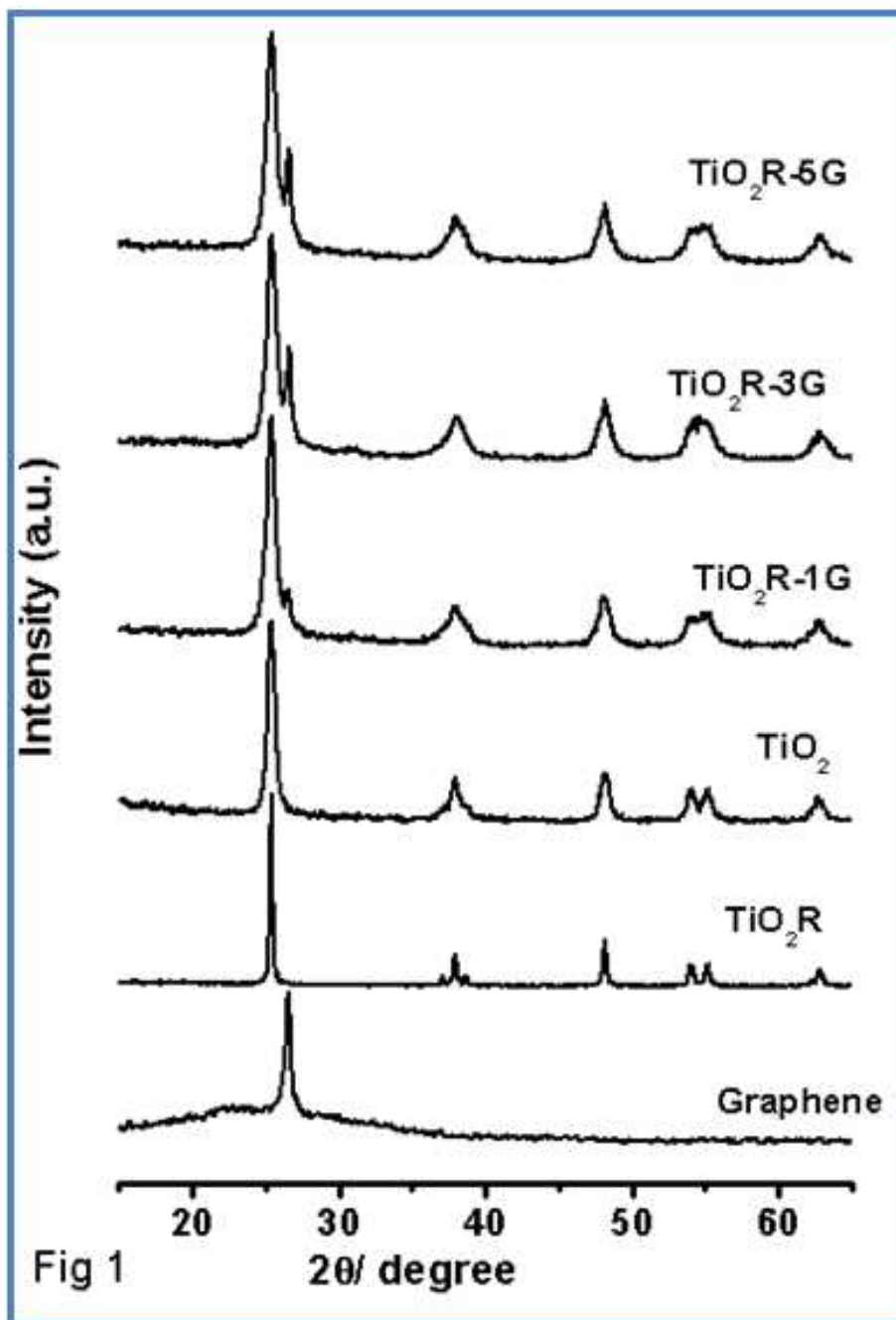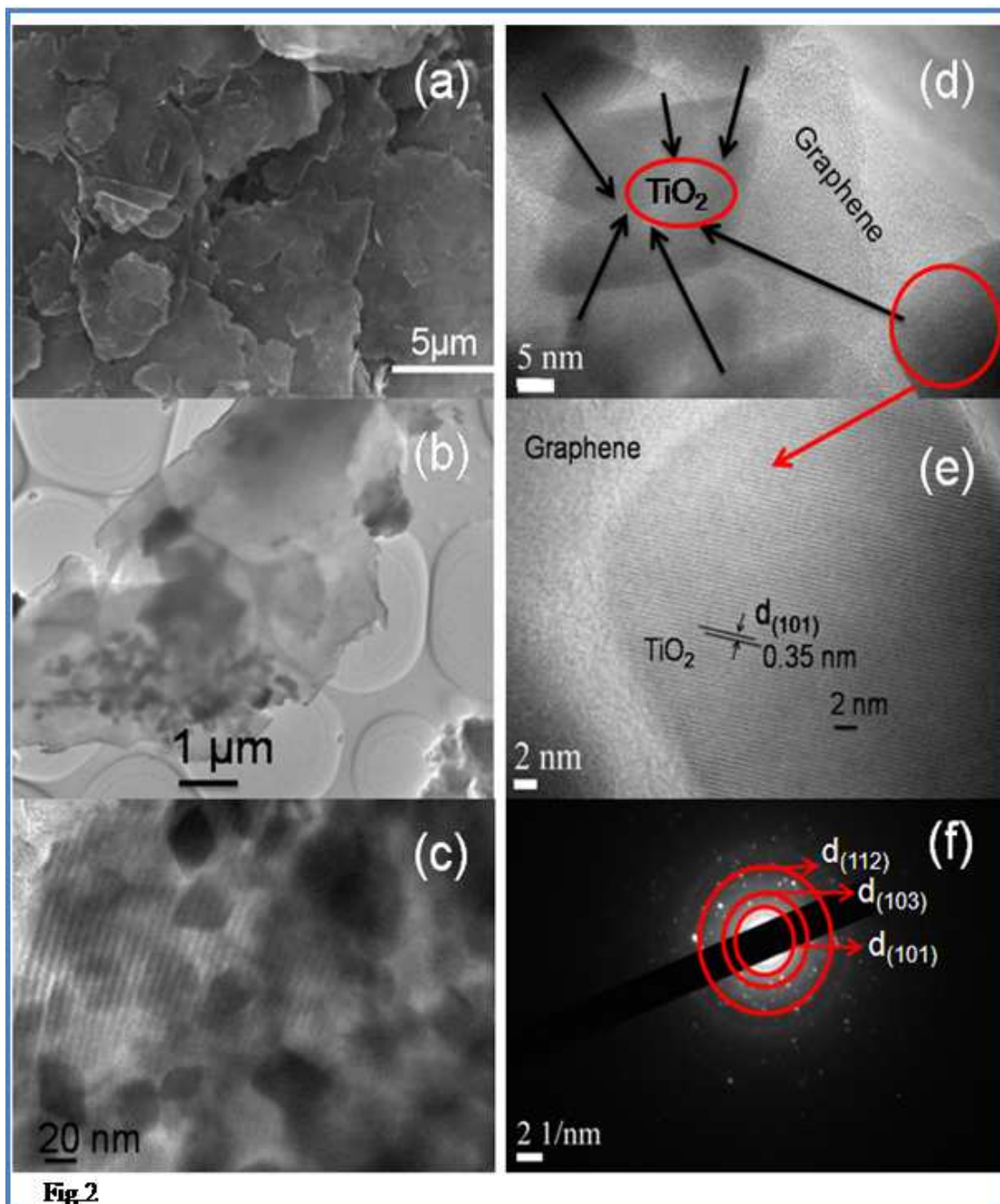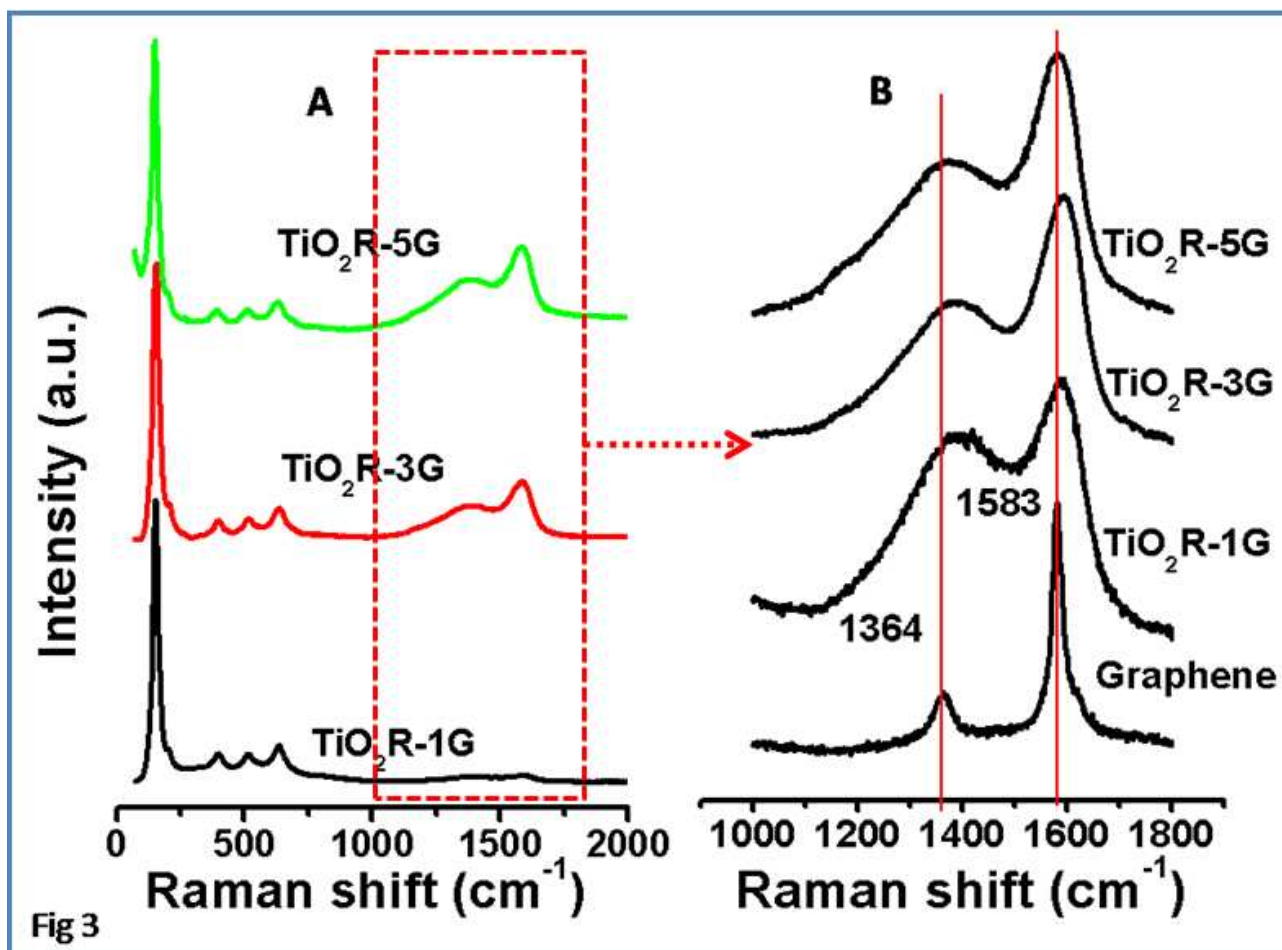
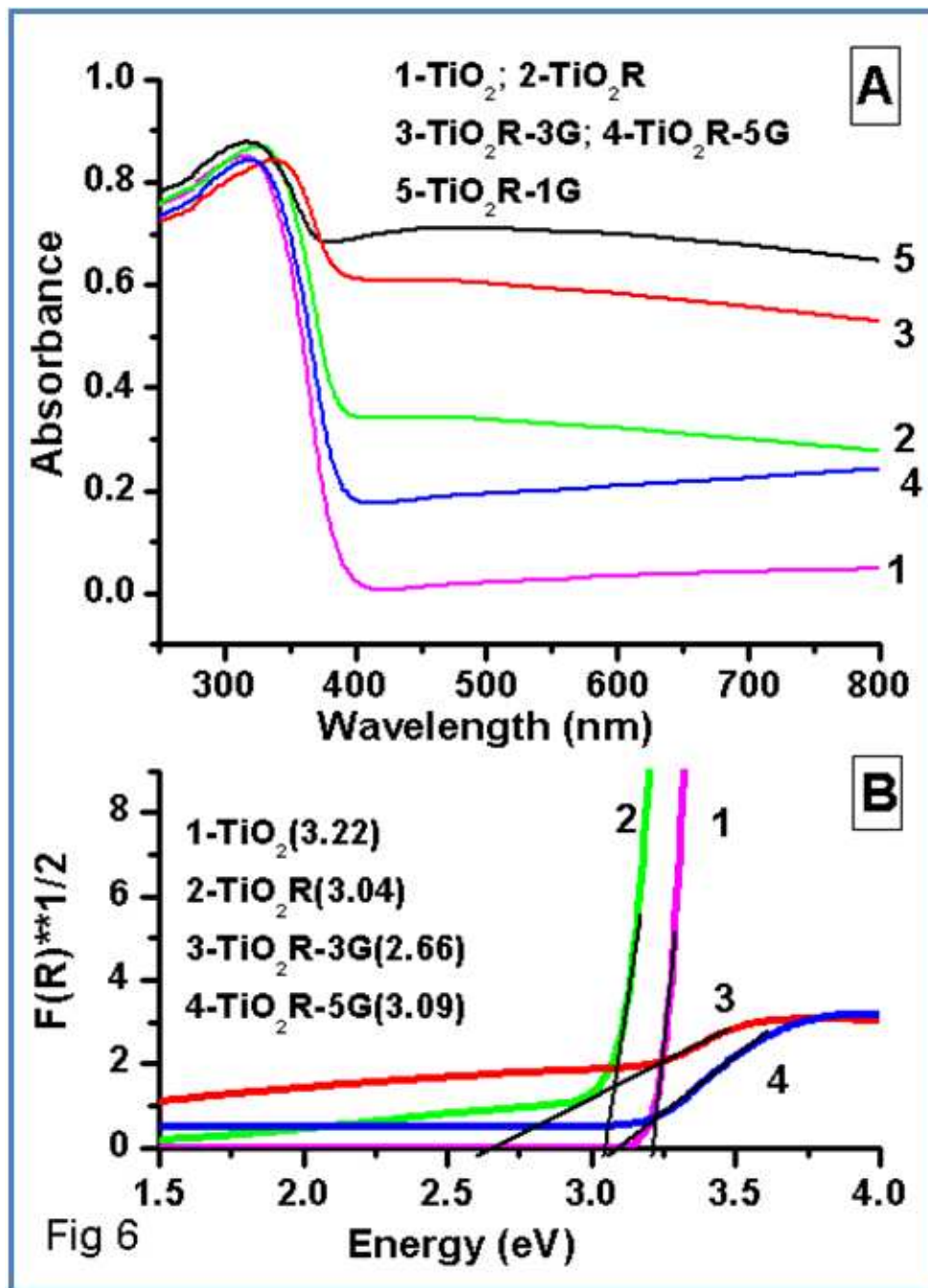Fig 1   2θ/ degree

Fig.1

Fig.2

Fig 3
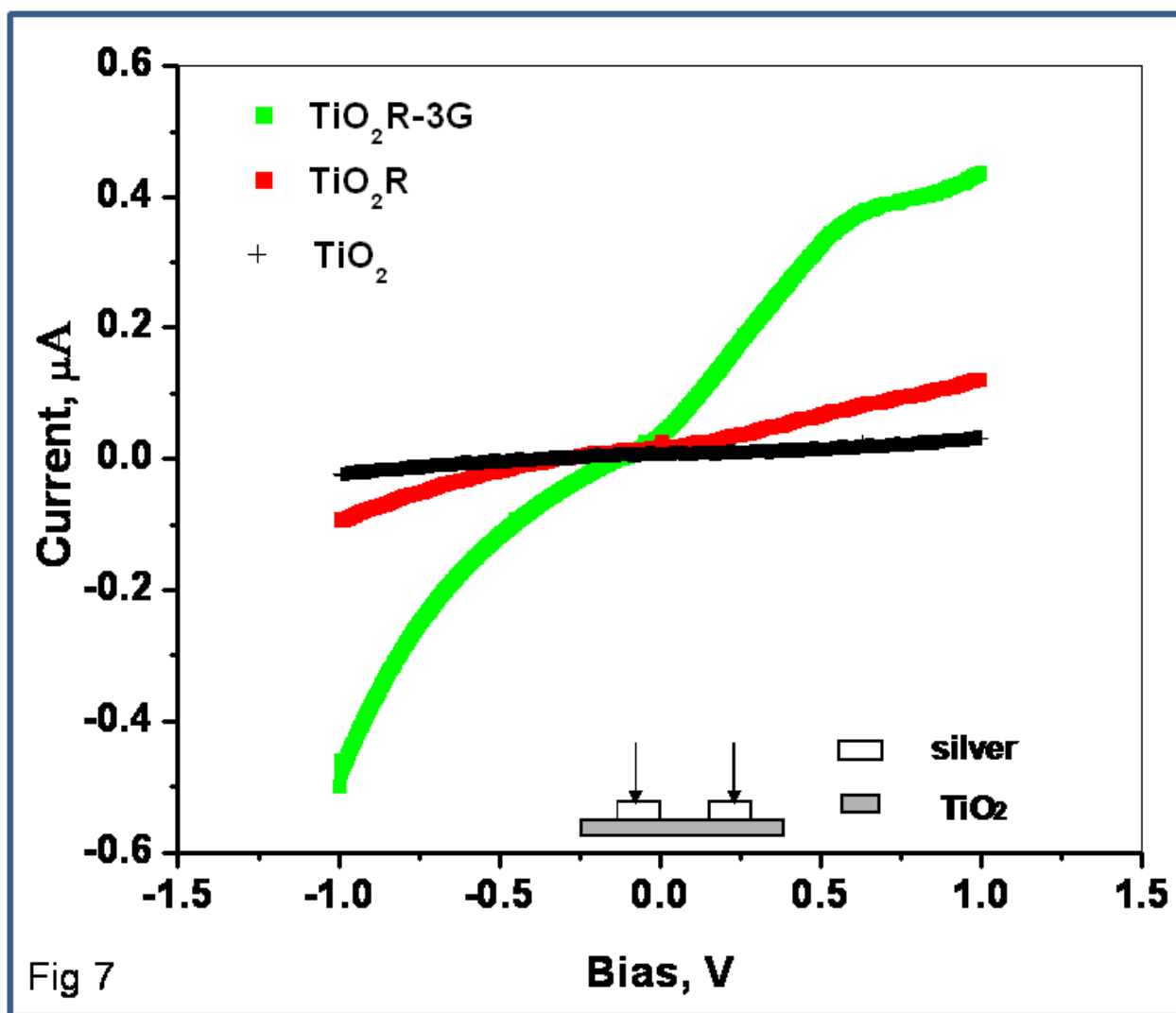
Fig.3
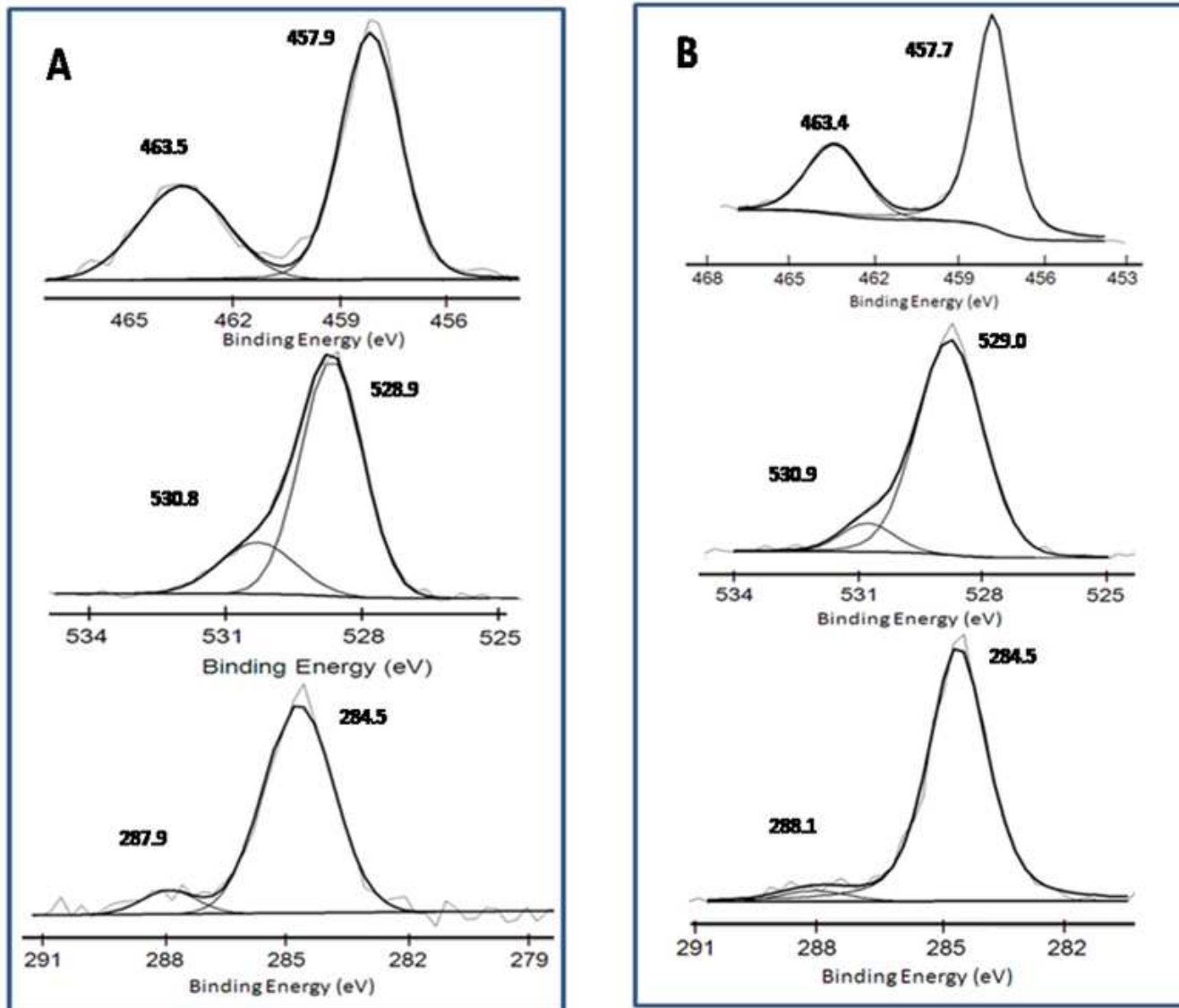
Fig 4
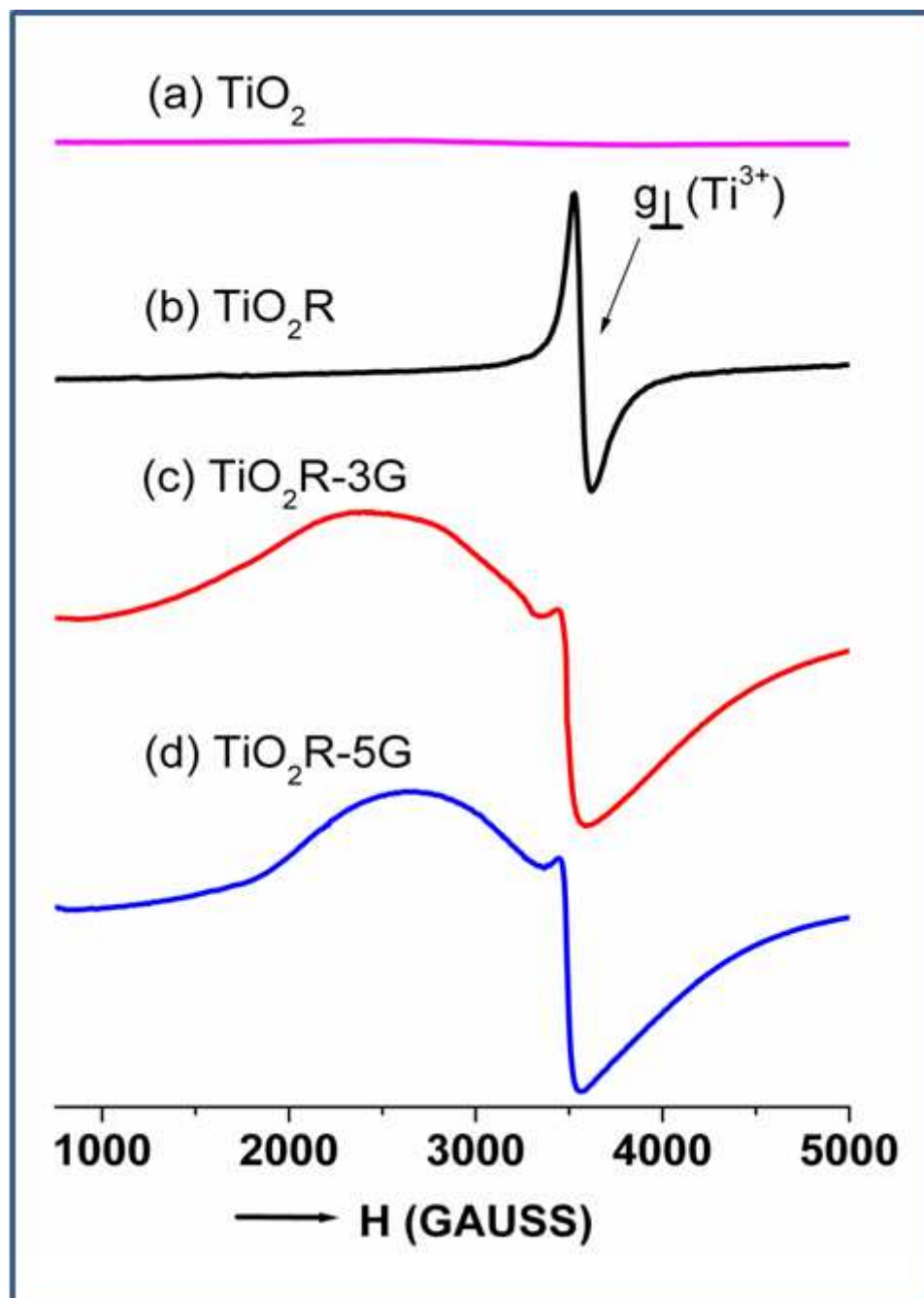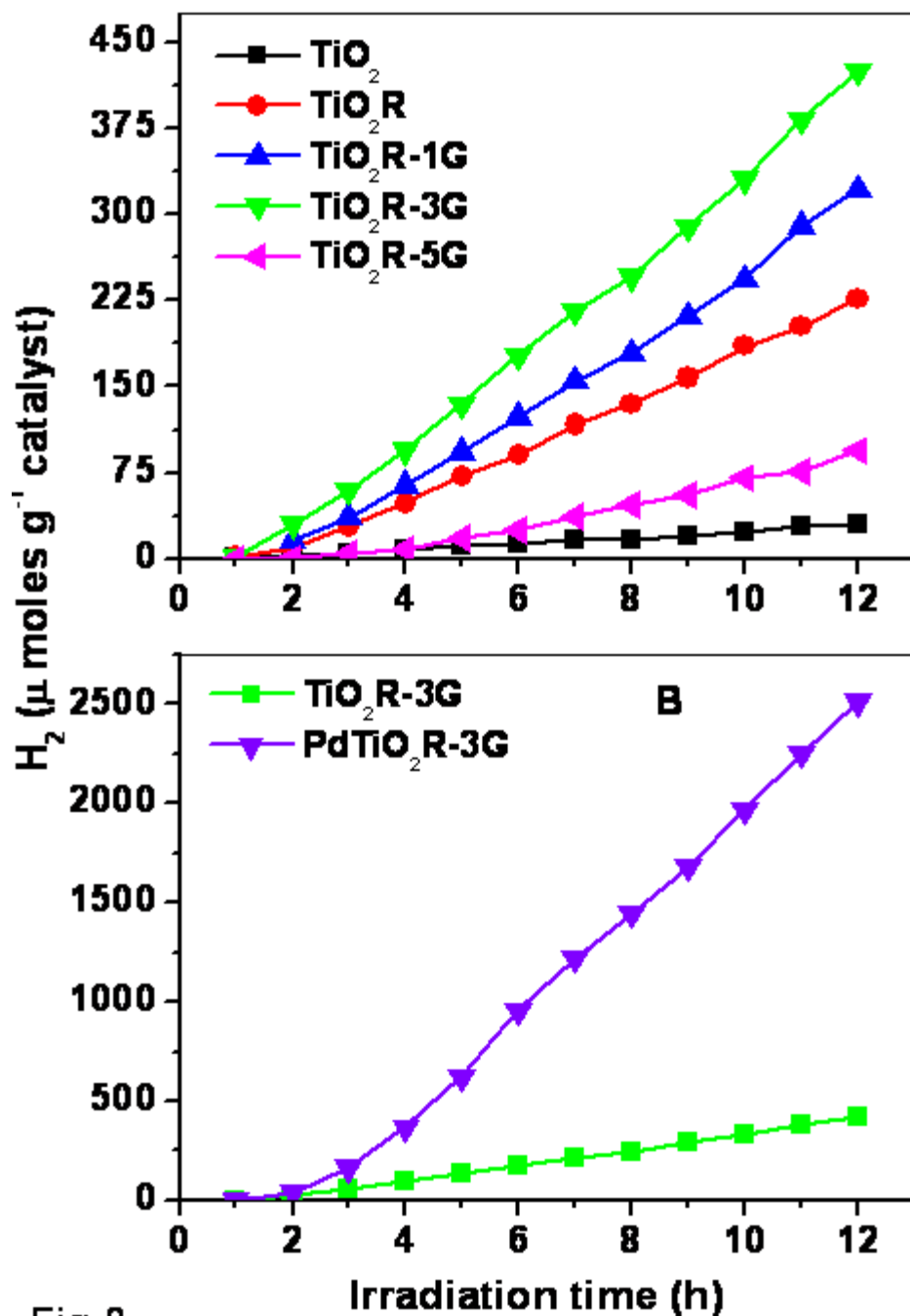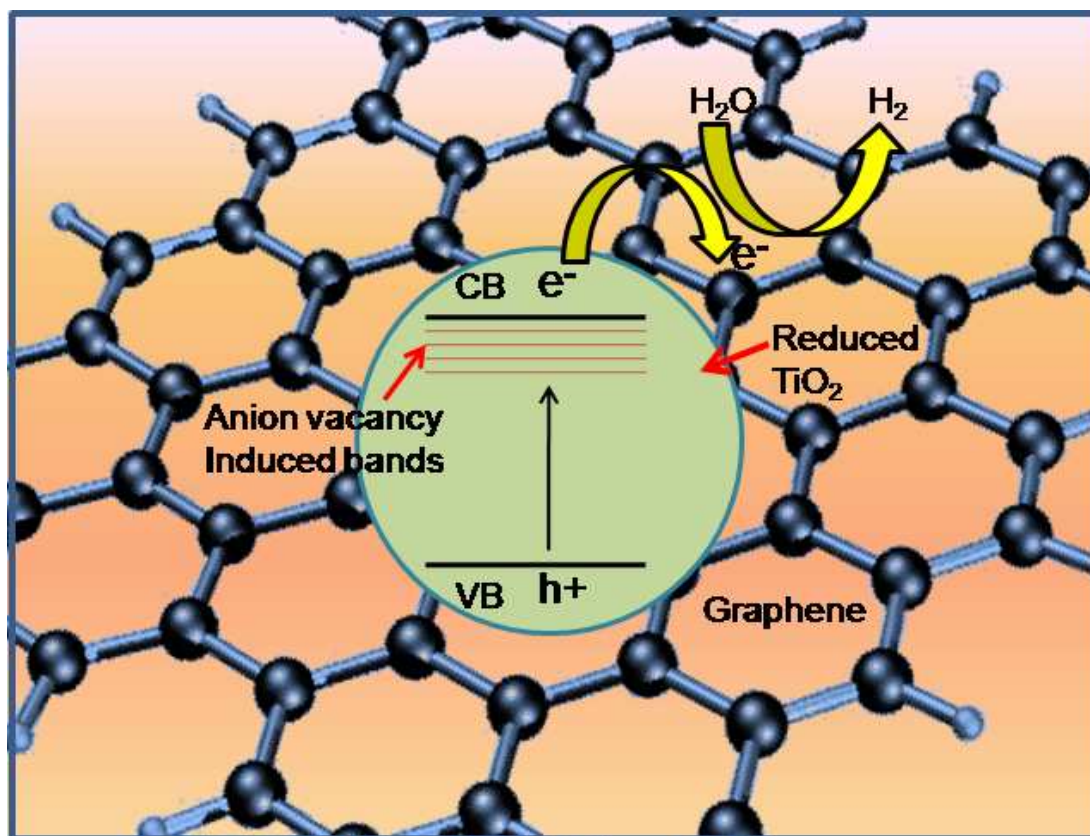
Fig.5

Fig.6

Fig 7

Fig.7

Fig 8

Fig. 9

Figure Captions

Fig. 1   Powder XRD patterns of graphene, TiO_2, TiO_2R and TiO_2R-G.

Fig. 2   SEM (a), TEM (b, c, d), HRTEM (e) images and SAED pattern (f) of TiO_2R-3G.

Fig. 3   Raman spectra of graphene and TiO_2R-G.

Fig. 4   Ti 2p, O 1s and C 1s X-ray photoelectron spectra of (A)TiO_2R and (B) TiO_2R-3G.

Fig. 5   EPR spectra of (a) Unreduced TiO_2 (b) TiO_2R, (c) TiO_2R-3G and (d) TiO_2R-5G.

Fig. 6   A. UV-visible DRS of TiO_2, TiO_2R and TiO_2R-G; B. Modified KM function plotted

against hν for TiO_2, TiO_2R and TiO_2R-G; the numbers given in brackets is the bandgap values.

Fig. 7   I-V plots of TiO_2, TiO_2R and TiO_2R-3G.

Fig. 8   Photocatalytic activity for hydrogen generation as a function of irradiation time (A) TiO_2,

TiO_2R and TiO_2R-G composites, (B) TiO_2R-3G and Pd-TiO_2R-3G. Reaction conditions:

50 mg catalyst suspended in 25 cm^3 of water and methanol mixture in 4:1 ratio by

volume; light source: Ordinary day light fluorescent lamp (total 36x8=288 watts).

Fig. 9   Schematic illustration of the charge separation process in TiO_2R-G composites.